Xenon Biosensor

DOI: 10.1002/anie.201300170

Molecular Imaging of Cancer Cells Using a Bacteriophage-Based ^{129}Xe NMR Biosensor**

*Krishnan K. Palaniappan, R. Matthew Ramirez, Vikram S. Bajaj, David E. Wemmer, Alexander Pines, and Matthew B. Francis**

The accurate detection and localization of clinically relevant biomarkers in vivo is a great challenge for molecular imaging, requiring high sensitivity and molecular specificity.[1] This is particularly true for screening applications, where the ability to image disease progression non-invasively could improve patient outcome. Magnetic resonance imaging (MRI) is a ubiquitous, non-invasive imaging technique with sub-millimeter spatial resolution,[2] but its use in molecular imaging has been limited by its poor sensitivity when imaging molecules other than water.[1,3] This has led to the development of contrast agents and MRI methods that improve sensitivity by modulating the local magnetic environment of protons in water, including gadolinium chelators,[4] iron-oxide particles,[5] and chemical exchange saturation transfer (CEST).[6] More recently, approaches that use hyperpolarized ^{13}C, ^{3}He, and ^{129}Xe nuclei have been developed and used in clinical studies.[7]

In the experiments below, we used xenon (Xe) as a sensor medium. Xe is an attractive option for MRI-based molecular imaging because it is chemically inert, has low toxicity,[8] is soluble in water and tissue, and can be hyperpolarized (hp) to increase its signal more than 10000-fold.[9] Thus, even low concentrations of dissolved Xe give an NMR signal comparable to that of water, and there is no Xe background in vivo. These favorable properties of Xe MRI have already been demonstrated in humans after inhalation of hp ^{129}Xe gas.[10]

Molecular imaging agents that leverage these characteristics, generally called Xe biosensors, have been developed.[11] They consist of a Xe-binding host molecule, commonly cryptophane-A (CryA),[12] attached to targeting groups for localization.[13] Xenon bound by CryA (Xe@CryA) has a distinct chemical shift apart from that of aqueous Xe (Xe@water).[11] Its rapid and reversible encapsulation is the basis of an indirect detection scheme in which the small Xe@CryA spin pool is saturated by frequency-selective radiofrequency (RF) pulses and transferred by exchange to the larger Xe@water spin pool, an example of amplification by CEST. This results in a decrease in the signal relative to a control experiment (Figure 1a).[11b] Combined with the signal enhancement of hyperpolarization, Xe biosensors can achieve the detection thresholds necessary for molecular imaging.[14] To improve the sensitivity further we used multivalent systems in which many CryA hosts are assembled onto a single carrier molecule, a concept initially applied with paramagnetic relaxation and CEST agents.[15] We have demonstrated this strategy for Xe biosensors with branched dendrimers[16] and viral capsids,[17] producing constructs that were detectable by hyperCEST at sub-picomolar concentrations.

In previous studies of Xe biosensors biological binding events were measured in solution. This was first achieved with biotin-functionalized biosensors binding streptavidin beads,[11,14a,18] and subsequently with the detection of DNA hybridization,[19] enzymatic cleavage by matrix metalloproteinase-7,[20] ligand binding to human carbonic anhydrase[21] and an $\alpha_{2b}\beta_3$ integrin,[22] and peptide complex formation with a major histocompatibility complex protein.[23] Once the cellular compatibility of Xe biosensors was established,[22,24] ^{129}Xe NMR spectroscopy was performed with cells after targeting them with micromolar concentrations of a transferrin-functionalized biosensor.[25] While that study detected biosensor binding by measuring the Xe@CryA chemical shift, non-specific binding was also observed.

Here, we report a multivalent Xe biosensor that uses single-chain antibodies to target cell surface biomarkers. We further specifically demonstrate its ability to specifically recognize these biomarkers in living cells and at concentrations required for molecular imaging. To accomplish this, we used fd filamentous bacteriophage that display single-chain antibody variable fragments (scFvs) on their minor coat proteins (p3, Figure 1b).[26] The rod-like body of the fd phage, which has 4200 identical copies of the major coat protein (p8), can be modified with proteins or synthetic molecules to create new materials.[27] Additionally, through the use of phage display techniques, filamentous phage that display proteins as

[*] Dr. K. K. Palaniappan,[+] R. M. Ramirez,[+] Dr. V. S. Bajaj, Prof. Dr. D. E. Wemmer, Prof. Dr. A. Pines, Prof. Dr. M. B. Francis
Department of Chemistry, University of California
Berkeley, CA 94720-1460 (USA)
E-mail: mbfrancis@berkeley.edu

R. M. Ramirez,[+] Dr. V. S. Bajaj, Prof. Dr. A. Pines, Prof. Dr. M. B. Francis
Materials Sciences Division
Lawrence Berkeley National Laboratory
Berkeley, CA 94720-1460 (USA)

Prof. Dr. D. E. Wemmer
Physical Biosciences Division
Lawrence Berkeley National Laboratory
Berkeley, CA 94720-1460 (USA)

[+] These authors contributed equally to this work.

[**] This work was supported by grants from the U.S. Department of Defense Cancer Research Program (grant number BC016995, M.B.F.) and by the U.S. Department of Energy, Office of Basic Energy Sciences, Division of Materials Science and Engineering under contract number DE-AC02-05CH112 (A.P.).

Supporting information for this article is available on the WWW under http://dx.doi.org/10.1002/anie.201300170.

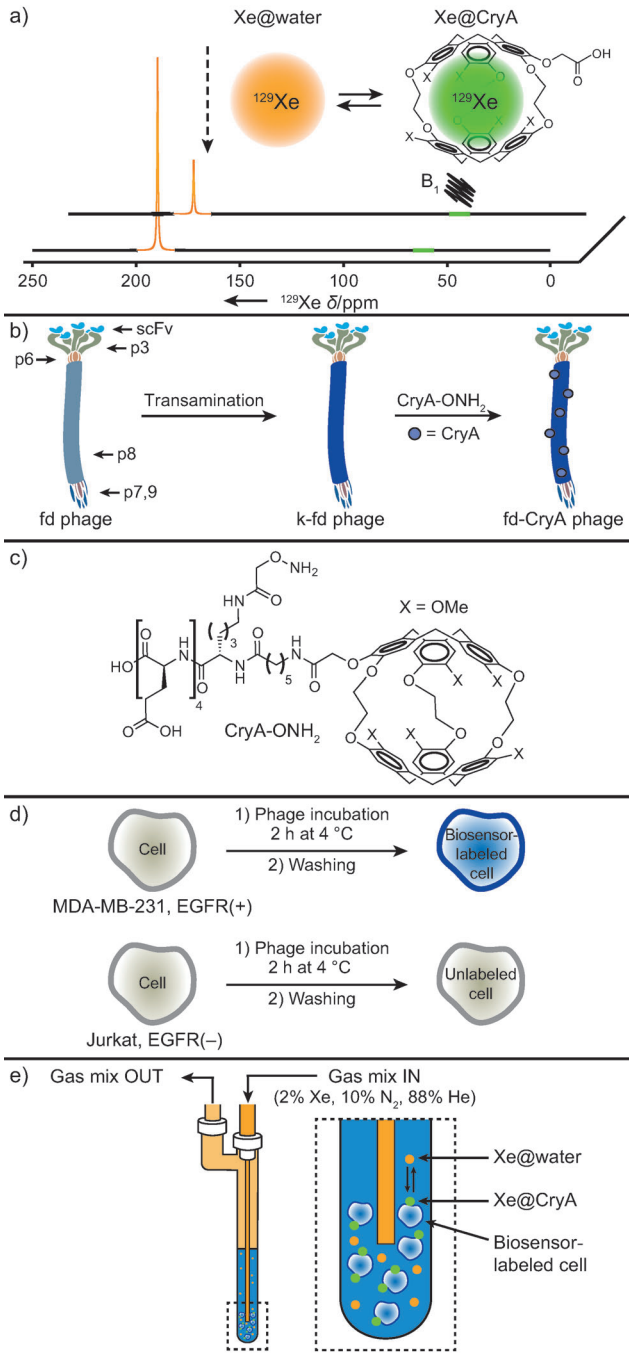

Figure 1. a) The exchange of Xe between solution and CryA cages results in a decrease in the Xe@water signal upon application of a frequency-selective saturation pulse (B_1) at the chemical shift of Xe@CryA. b) To modify fd phage with CryA, the phage were first transaminated to introduce ketones at the N-termini of their p8 coat proteins (k-fd) and then incubated with CryA-ONH_2 to produce fd-CryA constructs. c) The chemical structure of aminoxy-functionalized cryptophane-A cage (CryA-ONH_2). d) For cell-labeling experiments, MDA-MB-231 (EGFR+) and Jurkat (EGFR-) cells were incubated with phage constructs for 2 h at 4 °C. After removing unbound phage, cells were analyzed by flow cytometry, microscopy, or ^{129}Xe NMR spectroscopy. e) Live cell Xe NMR experiments were performed in a modified 5 mm NMR tube that allowed for gas flow.

extensions of their coat proteins can be evolved to bind small molecules, proteins, and metal ions with high affinity and selectivity.[28] In this case, the scFvs recognized either the epidermal growth factor receptor (EGFR) or, as a negative control, botulinum toxin serotype A (BONT), with nano- to sub-nanomolar affinity.[29] Our biosensors were designed to target EGFR because EGFR is a cell surface receptor that is highly expressed in a variety of solid tumors, including breast cancer.[30] EGFR expression levels can also be used to predict cancer progression,[31] making it an ideal cellular target for both therapeutics and molecular imaging applications.

Synthetic components can be introduced onto the surface of filamentous phage through several bioconjugation strategies.[27b,32] Recently, we applied an N-terminal specific bioconjugation method for modifying filamentous phage containing scFvs with fluorophores and polymers. We further verified that the modified phages maintained their cell-binding properties.[27c,33] Additionally, we used the same chemistry to modify non-targeted M13 filamentous phage with CryA to test the feasibility of using filamentous phage as a Xe biosensor, and demonstrated that the sensitivity of phage-grafted CryA groups was equivalent to that of free CryA.[17b] Based on this success, we used the same chemistry to construct a targeted fd-based Xe biosensor (Figure 1 b). First, the N-termini of the coat proteins were transaminated using pyridoxal 5′-phosphate to introduce ketone groups. After the ketone-labeled fd phage (k-EGFR and k-BONT) were purified, oxime ligation proceeded with an aminooxy-functionalized CryA-peptide (Figure 1 c, for synthesis see Figure S1 in the Supporting Information). After 22 h at RT, the resulting fd-CryA biosensors (i.e., EGFR-CryA and BONT-CryA) were purified by gel filtration and characterized by reverse-phase HPLC (Figure S2). On average, the biosensors were about 8% modified with CryA cages, corresponding to about 330 copies per phage.

To verify that fd-CryA biosensors retained their binding specificity, the modified phage were incubated with either MDA-MB-231 cells (a breast cancer cell-line with high EGFR expression) or Jurkat cells (T-cells with low EGFR expression). The bound phage were fluorescently stained using an anti-fd bacteriophage antibody (Figure 1 d) and characterized by flow cytometry and confocal microscopy (Figure 2). All anti-EGFR phage constructs displayed a high binding specificity to MDA-MB-231 cells, with little-to-no non-specific binding to Jurkat cells (Figure 2 a, for representative dot plots and gating data see Figures S3 and S4). Additionally, the negative control anti-BONT phage constructs showed low binding to MDA-MB-231 cells, indicating that the CryA modification did not produce significant non-specific binding. Fluorescence microscopy revealed predominantly cell-surface binding with minimal cell internalization or non-specific binding (Figure 2 b and Figure S5). Having confirmed the binding specificity of the EGFR-CryA biosensor, we proceeded to characterize the hyperCEST response of biosensor-labeled cells with ^{129}Xe NMR spectroscopy.

Xe gas was introduced into cell solutions using a continuous-flow bubbling system (illustrated in Figure 1 e).[34] While this method facilitated the rapid dissolution of Xe gas, bubbling through a solution of cells introduced complications

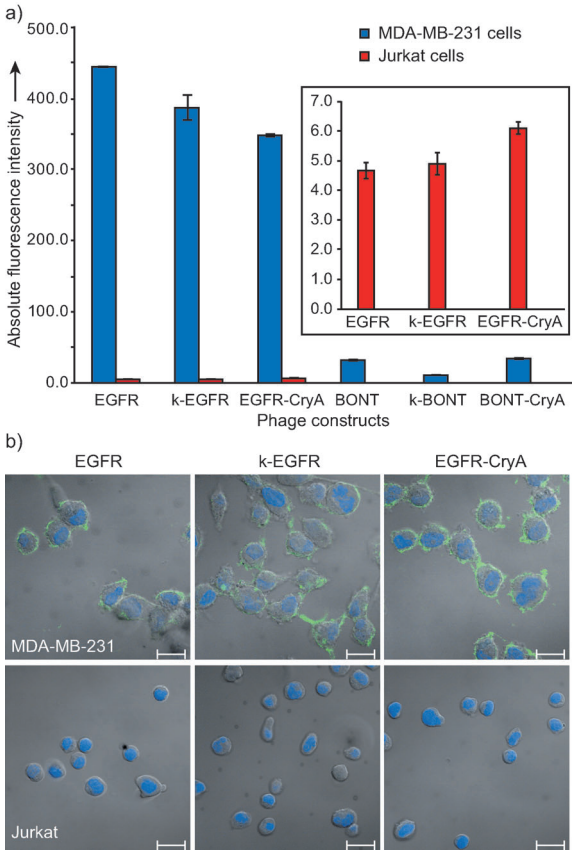

Figure 2. EGFR-CryA phage maintain their cell-binding specificity. a) Flow cytometry indicated that all three EGFR phage constructs bound similarly to MDA-MB-231 cells (EGFR+), but they did not bind to Jurkat cells (EGFR-). In contrast, none of the three BONT phage constructs bound to MDA-MB-231 cells, indicating that the CryA modification did not produce non-specific binding. The inset is an enlargement of the Jurkat cell-binding data. Shown is a representative experiment from three biological replicates, each performed in triplicate. Error bars represent the standard deviation. b) Confocal microscopy showed that all three EGFR phage constructs bound to MDA-MB-231 cell surfaces, but were not bound to Jurkat cells. Representative merged images are shown using DAPI (blue) to label cell nuclei and FITC (green) to label the phage (see Figure S5 for each channel); the scale bars are 20 μm.

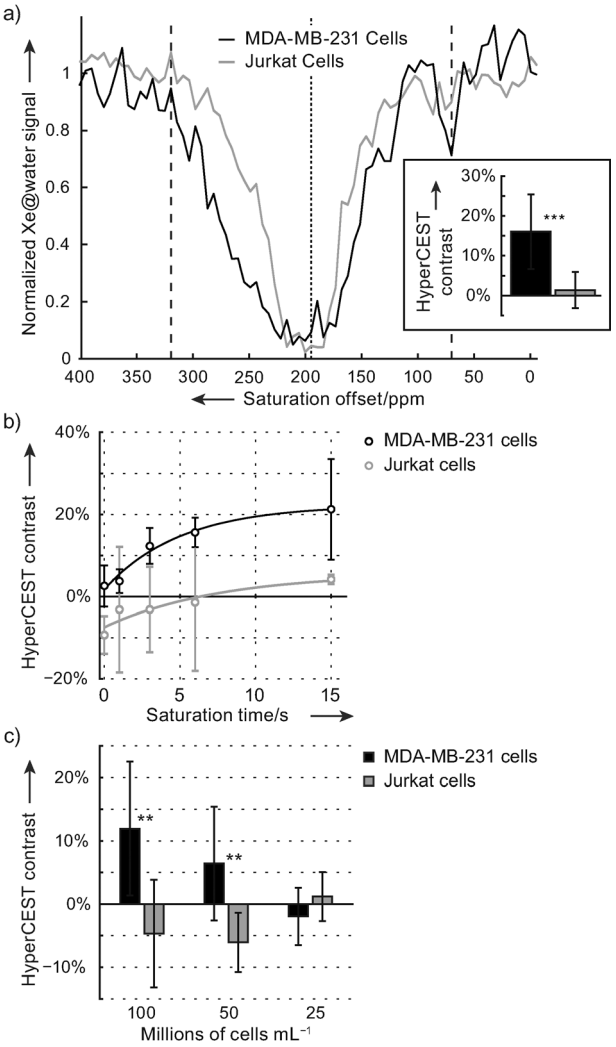

Figure 3. The hyperCEST response of MDA-MB-231 and Jurkat cells labeled with the EGFR-CryA biosensor is specific to MDA-MB-231 cells, an EGFR positive cell line. a) Comparison of the saturation response profiles indicated that the EGFR-CryA biosensor was bound only by MDA-MB-231 cells, as evidenced by the dip at 70 ppm. Saturation consisted of a train of 500 Hz bandwidth dSNOB pulses totaling 10 s. Dashed lines indicate the offset frequencies used for saturation pulse trains in b) and c), whereas the dotted line shows the chemical shift of Xe@water. Inset: The hyperCEST contrast of each sample was quantified using the same dSNOB pulse train. b) The hyperCEST contrast was measured as a function of saturation duration using a train of 500 Hz bandwidth dSNOB pulses. Longer saturation times produced more contrast for the MDA-MB-231 sample. The solid line represents an exponential fit to the data. c) The cellular detection limit was explored using a higher-intensity, 1000 Hz bandwidth dSNOB pulse train. All plots show a mean contrast ± standard deviation for either 4 (line graphs) or 10 (bar graphs) replicates, except for the saturation response profiles (a), which were collected in a single shot. *** $P < 0.001$, ** $P < 0.01$.

including foaming and the mechanical stress of bubbles on cell integrity. Therefore, we assessed the viability of Jurkat and MDA-MB-231 cells over the time course of a typical set of NMR experiments. We found that while most of the Jurkat cell membranes remained intact, a significant number of MDA-MB-231 cells had compromised membranes within 90 minutes (Figure S6). Taking into account both cell viability and the propensity for sample foaming, we limited the duration of bubbling experiments to 70 minutes for any one solution of cells.

^{129}Xe NMR spectroscopy was performed with live cells at a concentration of 100 million cells mL^{-1} (Figure 1d and e). After unbound biosensor was rinsed away, the saturation profile of each sample was recorded by measuring the Xe@water signal as a function of the frequency of a RF saturation pulse train to reveal the presence of any Xe populations exchanging with Xe@water (Figure 3a). As expected, a region of saturation centered at 70 ppm, characteristic of Xe@CryA, was seen with MDA-MB-231 cells. The same feature was not observed with Jurkat cells, establishing the specificity of the EGFR–CryA biosensor. To verify that both cells were incubated with comparable concentrations of the EGFR–CryA biosensor, cell labeling solutions were

analyzed by hyperCEST in the same manner and each showed a strong saturation at 70 ppm, confirming the presence of the EGFR–CryA biosensor (Figure S9).

The contrast of the cell solutions was quantified with a 500 Hz bandwidth dSNOB pulse train 10 s in duration (Figure 3a, inset). While the MDA-MB-231 cell solution exhibited a $16.0 \pm 9.4\,\%$ contrast, the Jurkat cell solution exhibited essentially no contrast ($1.4 \pm 4.6\,\%$). Contrast was also measured as a function of saturation time using the same saturation pulse scheme (Figure 3b). A saturation duration of 3 s was sufficient to generate $12.3 \pm 4.4\,\%$ in the solution of MDA-MB-231 cells, but increasing that time provided marginal benefits. For instance, doubling the saturation length to 6 s yielded just $15.6 \pm 3.6\,\%$, and a 15 s saturation period produced only $21.3 \pm 12.3\,\%$, less than two times the contrast of a pulse train 5 times shorter.

To further characterize biosensor-labeled cells and estimate the cellular detection limit for biosensor-labeled MDA-MB-231 cells, contrast was measured as a function of the cell concentration with a series of successive dilutions (Figure 3c). A saturation pulse train of higher intensity (1000 Hz bandwidth) was used in an effort to create as much contrast as possible. Though the overall contrast was low and somewhat variable ($6.4 \pm 9.0\,\%$), a statistically significant difference in contrast ($P < 0.01$) between the two samples was generated at concentrations as low as 50 million cells mL^{-1}; we envision that this limit will be lowered with improvements to the experimental setup. For example, the sensitivity can be improved by two orders of magnitude by the isotopic enrichment of Xe, by its separation from the buffer gas mixture used for polarization, and by increasing its polarization.[35] Additionally, the dissolution of hp ^{129}Xe through gas-exchange membranes, as opposed to bubbling, should result in a more uniform signal distribution while reducing harmful perturbations of the cells.[36]

The negative contrast observed in the Jurkat cell solution (Figure 3c) was the result of the broad, asymmetric response profile to the symmetric RF saturation pulse train. This phenomenon was also observed with unlabeled Jurkat and MDA-MB-231 cells, but was not seen in the media alone (Figure S10), suggesting the existence of another Xe population in the regime of intermediate-to-fast exchange with Xe@water. This could be Xe associated with cell membranes (Xe@cell). Although a distinct Xe@cell peak was not observed in the direct spectra (Figure S11), unique chemical shifts have been reported for xenon associated with cells,[25,37] and the Xe@water linewidth observed for cell solutions is consistent with exchange broadening. Furthermore, fitting a linear combination of Gaussian distributions to these data reveals two Xe populations, (i.e., Xe@water and Xe@cell; Figure S12).

In this study, we have successfully created a targeted, viral capsid-based Xe biosensor that recognizes the EGF receptor with high specificity. We have also demonstrated its use for live-cell ^{129}Xe NMR spectroscopy with hyperCEST detection. Importantly, our modular design of the biosensor makes it a versatile contrast agent suitable for many molecular imaging applications. For instance, because we have shown that fd phage with scFvs maintain their binding specificity after modification, we can access Xe biosensors for a variety of targets using phage display techniques. Additionally, beyond CryA cages, we can introduce virtually any aminooxy-functionalized molecule, including fluorophores for multimodal MR/optical imaging, and polyethylene glycols for enhanced in vivo pharmacodynamics. In the future, we intend to leverage this potential to build Xe biosensors that can be used for in vivo MRI of lung and other cancers.

Experimental details are available in the Supporting Information.

Received: January 8, 2013
Revised: February 9, 2013
Published online: March 28, 2013

Keywords: cancer cells · NMR imaging · protein bioconjugation · viral capsids · xenon

[1] T. F. Massoud, S. S. Gambhir, *Genes Dev.* **2003**, *17*, 545–580.
[2] J. M. Tyszka, S. E. Fraser, R. E. Jacobs, *Curr. Opin. Biotechnol.* **2005**, *16*, 93–99.
[3] D. E. Sosnovik, R. Weissleder, *Curr. Opin. Biotechnol.* **2007**, *18*, 4–10.
[4] K. W. Y. Chan, W. T. Wong, *Coord. Chem. Rev.* **2007**, *251*, 2428–2451.
[5] J. W. M. Bulte, D. L. Kraitchman, *NMR Biomed.* **2004**, *17*, 484–499.
[6] M. Woods, E. W. C. Donald, A. D. Sherry, *Chem. Soc. Rev.* **2006**, *35*, 500–511.
[7] a) J. Kurhanewicz, R. Bok, S. J. Nelson, D. B. Vigneron, *J. Nucl. Med.* **2008**, *49*, 341–344; b) S. R. Hopkins, D. L. Levin, K. Emami, S. Kadlecek, J. S. Yu, M. Ishii, R. R. Rizi, *J. Appl. Physiol.* **2007**, *102*, 1244–1254; c) A. M. Oros, N. J. Shah, *Phys. Med. Biol.* **2004**, *49*, R105–R153.
[8] K. Kawakami, *Ann. Nucl. Med.* **1997**, *11*, 67–73.
[9] a) P. Berthault, G. Huber, H. Desvaux, *Prog. Nucl. Magn. Reson. Spectrosc.* **2009**, *55*, 35–60; b) T. G. Walker, W. Happer, *Rev. Mod. Phys.* **1997**, *69*, 629–642; c) B. M. Goodson, *J. Magn. Reson.* **2002**, *155*, 157–216.
[10] a) J. P. Mugler, B. Driehuys, J. R. Brookeman, G. D. Cates, S. S. Berr, R. G. Bryant, T. M. Daniel, E. E. deLange, J. H. Downs, C. J. Erickson, W. Happer, D. P. Hinton, N. F. Kassel, T. Maier, C. D. Phillips, B. T. Saam, K. L. Sauer, M. E. Wagshul, *Magnet. Reson. Med.* **1997**, *37*, 809–815; b) M. S. Albert, G. D. Cates, B. Driehuys, W. Happer, B. Saam, C. S. Springer, A. Wishnia, *Nature* **1994**, *370*, 199–201.
[11] a) M. M. Spence, S. M. Rubin, I. E. Dimitrov, E. J. Ruiz, D. E. Wemmer, A. Pines, S. Q. Yao, F. Tian, P. G. Schultz, *Proc. Natl. Acad. Sci. USA* **2001**, *98*, 10654–10657; b) M. M. Spence, E. J. Ruiz, S. M. Rubin, T. J. Lowery, N. Winssinger, P. G. Schultz, D. E. Wemmer, A. Pines, *J. Am. Chem. Soc.* **2004**, *126*, 15287–15294.
[12] a) J. Gabard, A. Collet, *J. Chem. Soc. Chem. Commun.* **1981**, 1137–1139; b) K. Bartik, M. Luhmer, J. P. Dutasta, A. Collet, J. Reisse, *J. Am. Chem. Soc.* **1998**, *120*, 784–791.
[13] O. Taratula, I. J. Dmochowski, *Curr. Opin. Chem. Biol.* **2010**, *14*, 97–104.
[14] a) L. Schroder, T. J. Lowery, C. Hilty, D. E. Wemmer, A. Pines, *Science* **2006**, *314*, 446–449; b) L. Schroder, T. Meldrum, M. Smith, T. J. Lowery, D. E. Wemmer, A. Pines, *Phys. Rev. Lett.* **2008**, *100*, 257603.
[15] a) M. T. Dedeo, D. T. Finley, M. B. Francis, *Prog Mol Biol Transl Sci* **2011**, *103*, 353–392; b) O. Vasalatiy, R. D. Gerard, P. Zhao, X. Sun, A. D. Sherry, *Bioconjugate Chem.* **2008**, *19*, 598–606.

[16] J. L. Mynar, T. J. Lowery, D. E. Wemmer, A. Pines, J. M. Frechet, *J. Am. Chem. Soc.* **2006**, *128*, 6334 – 6335.
[17] a) T. Meldrum, K. L. Seim, V. S. Bajaj, K. K. Palaniappan, W. Wu, M. B. Francis, D. E. Wemmer, A. Pines, *J. Am. Chem. Soc.* **2010**, *132*, 5936 – 5937; b) T. K. Stevens, K. K. Palaniappan, R. M. Ramirez, M. B. Francis, D. E. Wemmer, A. Pines, *Magn. Reson. Med.*, DOI: 10.1002/mrm.24371.
[18] T. J. Lowery, S. Garcia, L. Chavez, E. J. Ruiz, T. Wu, T. Brotin, J. P. Dutasta, D. S. King, P. G. Schultz, A. Pines, D. E. Wemmer, *ChemBioChem* **2006**, *7*, 65 – 73.
[19] V. Roy, T. Brotin, J. P. Dutasta, M. H. Charles, T. Delair, F. Mallet, G. Huber, H. Desvaux, Y. Boulard, P. Berthault, *ChemPhysChem* **2007**, *8*, 2082 – 2085.
[20] Q. Wei, G. K. Seward, P. A. Hill, B. Patton, I. E. Dimitrov, N. N. Kuzma, I. J. Dmochowski, *J. Am. Chem. Soc.* **2006**, *128*, 13274 – 13283.
[21] J. M. Chambers, P. A. Hill, J. A. Aaron, Z. Han, D. W. Christianson, N. N. Kuzma, I. J. Dmochowski, *J. Am. Chem. Soc.* **2009**, *131*, 563 – 569.
[22] G. K. Seward, Y. Bai, N. S. Khan, I. J. Dmochowski, *Chem. Sci.* **2011**, *2*, 1103.
[23] A. Schlundt, W. Kilian, M. Beyermann, J. Sticht, S. Gunther, S. Hopner, K. Falk, O. Roetzschke, L. Mitschang, C. Freund, *Angew. Chem.* **2009**, *121*, 4206 – 4209; *Angew. Chem. Int. Ed.* **2009**, *48*, 4142 – 4145.
[24] G. K. Seward, Q. Wei, I. J. Dmochowski, *Bioconjugate Chem.* **2008**, *19*, 2129 – 2135.
[25] C. Boutin, A. Stopin, F. Lenda, T. Brotin, J. P. Dutasta, N. Jamin, A. Sanson, Y. Boulard, F. Leteurtre, G. Huber, A. Bogaert-Buchmann, N. Tassali, H. Desvaux, M. Carriere, P. Berthault, *Bioorg. Med. Chem.* **2011**, *19*, 4135 – 4143.
[26] J. W. Kehoe, B. K. Kay, *Chem. Rev.* **2005**, *105*, 4056 – 4072.
[27] a) C. Mao, D. J. Solis, B. D. Reiss, S. T. Kottmann, R. Y. Sweeney, A. Hayhurst, G. Georgiou, B. Iverson, A. M. Belcher, *Science* **2004**, *303*, 213 – 217; b) I. Yacoby, I. Benhar, *Expert Opin. Drug Delivery* **2008**, *5*, 321 – 329; c) Z. M. Carrico, M. E. Farkas, Y. Zhou, S. C. Hsiao, J. D. Marks, H. Chokhawala, D. S. Clark, M. B. Francis, *ACS Nano* **2012**, *6*, 6675 – 6680.
[28] G. P. Smith, V. A. Petrenko, *Chem. Rev.* **1997**, *97*, 391 – 410.
[29] a) Y. Zhou, D. C. Drummond, H. Zou, M. E. Hayes, G. P. Adams, D. B. Kirpotin, J. D. Marks, *J. Mol. Biol.* **2007**, *371*, 934 – 947; b) Y. Zhou, J. D. Marks, *Methods Enzymol.* **2012**, *502*, 43 – 66; c) P. Amersdorfer, C. Wong, T. Smith, S. Chen, S. Deshpande, R. Sheridan, J. D. Marks, *Vaccine* **2002**, *20*, 1640 – 1648.
[30] J. J. Laskin, A. B. Sandler, *Cancer Treat. Rev.* **2004**, *30*, 1 – 17.
[31] R. I. Nicholson, J. M. Gee, M. E. Harper, *Eur. J. Cancer* **2001**, *37 Suppl 4*, S9 – 15.
[32] a) K. Li, Y. Chen, S. Li, H. G. Nguyen, Z. Niu, S. You, C. M. Mello, X. Lu, Q. Wang, *Bioconjugate Chem.* **2010**, *21*, 1369 – 1377; b) A. Merzlyak, S. Indrakanti, S. W. Lee, *Nano Lett.* **2009**, *9*, 846 – 852.
[33] J. M. Gilmore, R. A. Scheck, A. P. Esser-Kahn, N. S. Joshi, M. B. Francis, *Angew. Chem.* **2006**, *118*, 5433 – 5437; *Angew. Chem. Int. Ed.* **2006**, *45*, 5307 – 5311.
[34] S. I. Han, S. Garcia, T. J. Lowery, E. J. Ruiz, J. A. Seeley, L. Chavez, D. S. King, D. E. Wemmer, A. Pines, *Anal. Chem.* **2005**, *77*, 4008 – 4012.
[35] F. W. Hersman, I. C. Ruset, S. Ketel, I. Muradian, S. D. Covrig, J. Distelbrink, W. Porter, D. Watt, J. Ketel, J. Brackett, A. Hope, S. Patz, *Acad. Radiol.* **2008**, *15*, 683 – 692.
[36] D. Baumer, E. Brunner, P. Blumler, P. P. Zanker, H. W. Spiess, *Angew. Chem.* **2006**, *118*, 7440 – 7442; *Angew. Chem. Int. Ed.* **2006**, *45*, 7282 – 7284.
[37] C. Boutin, H. Desvaux, M. Carriere, F. Leteurtre, N. Jamin, Y. Boulard, P. Berthault, *NMR Biomed.* **2011**, *24*, 1264 – 1269.

